

RESEARCH ARTICLE

10.1029/2018JA025683

Key Points:

- Approximately 75% (34%) reduction in intense (moderate) storm occurrence rate during ascending and early descending phases of cycle 24 compared to cycle 23 is observed
- Cycle 24 showed no significant difference during equinoctial months for intense storms; however, cycle 23 exhibited equinoctial asymmetry
- ICMEs and/or their SH are identified to be the dominant drivers for intense storms during cycle 24 (~89%) and cycle 23 (~64)

Correspondence to:

R. Rawat,
rashmirs10@gmail.com

Citation:

Rawat, R., Echer, E., & Gonzalez, W. D. (2018). How different are the solar wind-interplanetary conditions and the consequent geomagnetic activity during the ascending and early descending phases of the solar cycles 23 and 24? *Journal of Geophysical Research: Space Physics*, 123, 6621–6638. <https://doi.org/10.1029/2018JA025683>

Received 17 MAY 2018

Accepted 14 JUL 2018

Accepted article online 24 JUL 2018

Published online 28 AUG 2018

How Different Are the Solar Wind-Interplanetary Conditions and the Consequent Geomagnetic Activity During the Ascending and Early Descending Phases of the Solar Cycles 23 and 24?

Rashmi Rawat^{1,2} , E. Echer¹ , and W. D. Gonzalez¹ 

¹National Institute for Space Research (INPE), São Paulo, Brazil, ²National Centre for Antarctic and Ocean Research, Vasco da Gama, India

Abstract The current work investigates the possible solar wind-interplanetary (SW-IP) drivers of geomagnetic storms during the longest period (ascending to early descending phases) of the ongoing solar cycle (24). We present a comparative analysis between the two consecutive solar cycles (SCs) 23 and 24. Both the cycles exhibited dual peak feature as observed in the smoothed sunspot numbers $SSN_{smoothed}$. For both the cycles, second peak in the $SSN_{smoothed}$ is higher than the first one as exhibited in the revised $SSN_{smoothed}$ version. During the entire interval between the ascending to early descending phases (December 2008 to December 2016) of SC-24, the southward directed B_z and the dawn-dusk electric field (E_y) were consistently weaker as compared to that during similar interval of SC-23 (May 1996 to July 2004). The geomagnetic field response represented by Dst index concurrently exhibited similar variation patterns during both the periods. A striking reduction in the intense storm occurrence rate by ~75% was observed during the considered period of the current solar cycle in comparison to the previous cycle. However, moderate storm occurrence was reduced only by 32% in SC-24 as compared to SC-23, which could be attributed to the dominance of corotating interaction regions during SC-24. No significant difference is found between the intense storm rates around the vernal and autumnal equinoxes in cycle 24, whereas distinct autumnal equinoctial dominance is evident for cycle 23. Further, within each cycle, there is no significant difference in the moderate storm rates around vernal and autumnal equinoxes.

1. Introduction

The sunspot numbers (SSNs) and areas are used as proxies to assess the solar activity evolution. On an average, the sunspot cycle and thus the solar activity exhibit a periodicity of 11 years known as the Schwabe cycle (Schwabe, 1844). The solar cycle (SC) is produced by the solar dynamo within the Sun and hence is magnetic in nature. Each sunspot cycle has three typical phases. The period characterized by an increase in SSNs, their groups and areas are designated as the ascending phase, followed by the maximum phase, which is distinguished by maximization of SSNs, groups, and areas. Eventually, a steady decline in the number of sunspots marks the declining phase of the cycle. The sunspot cycles are known to exhibit double peaked structure during the maximum activity period. First reporting of the dual peak feature was made by Gnevyshev (1963, 1967) for the SC-19, based on the 530.3-nm coronal line observations. The interval between the two peaks when the SSNs diminish is referred as the *Gnevyshev Gap* (GG; Storini & Pase, 1995). Antalova and Gnevyshev (1965) affirmed that Gnevyshev (1963) conclusions remained unchanged for the other sunspot cycles as well. For this, Antalova and Gnevyshev (1965) superposed the sunspot curves of eight sunspot cycles from 1874 to 1962 and obtained that there are always two maxima in the sunspot cycle. The double peak characteristic of the SC is associated with the sunspots in northern and southern solar hemispheres resulting from the global reorganization of the solar magnetic fields (Feminella & Storini, 1997; Norton & Gallagher, 2010; Storini et al., 2003).

Different phases of the SC witness diverse solar emissions like coronal mass ejections (CMEs), solar flares, and high-speed streams (HSS) that emanate from the coronal holes. Typically, the maximum phase is dominated by CMEs and solar flares. In contrast, the ascending and descending phases are dominated by HSS, which form the corotating interaction regions (CIRs) at their leading edges where they collide with the preceding

slower solar wind (Tsurutani & Gonzalez, 1997). The interplanetary counterparts of CMEs are known as interplanetary coronal mass ejections (ICMEs). ICMEs with flux rope structures are called as magnetic clouds (MCs). The MCs are characterized by high magnetic field, abnormally low proton temperature, large rotation of field, and low plasma beta (Burlaga et al., 1981). Dominance of these different solar wind-interplanetary (SW-IP) drivers during various phases of SC leads to varying intensity of geomagnetic activity. The geoeffectiveness of these interplanetary structures is measured in terms of the intensity of geomagnetic activity in correspondence to the solar wind and interplanetary magnetic field (IMF) behavior exhibited by the structures. It is well established that IMF B_z plays a crucial role for the efficient energy transfer from the solar wind into the magnetosphere through the magnetic reconnection process (Dungey, 1961; Gonzalez et al., 1994). Further, dawn-to-dusk component of the interplanetary electric field ($E_y = V_x \times B_z$), where V_x is the x component of V_{sw} , plays a pivotal role for the ring current injection during geomagnetic storms (Burton et al., 1975; Kan & Lee, 1979; Rawat et al., 2010).

ICMEs are predominant drivers of nonrecurrent intense to severe geomagnetic activity, primarily due to the presence of large southward directed B_z within them (Echer et al., 2008; Gonzalez et al., 1999, 2007; Zhang et al., 2007). CIRs, on the other hand, generally lead to recurrent moderate (Alves et al., 2006; Yermolaev et al., 2012) and sometimes intense activity (Richardson et al., 2006) generally driven by the southward fields associated with Alfvénic fluctuations in the IMF. The current SC is 24th that commenced in December 2008 after a deep solar minimum following the SC-23 (Tsurutani et al., 2011). It would be extremely interesting to compare the various activity levels during both the SCs. Several studies have been carried out discussing the deep solar minimum and the ongoing SC (e.g., Gopalswamy et al., 2015; Kilpua et al., 2014; Lepping et al., 2015; Richardson, 2013; Richardson & Cane, 2012b; Shanmugaraju et al., 2015). Richardson and Cane (2012b) and Richardson (2013) discussed the solar wind and geomagnetic activity over several cycles (1964–2011) and SC-24, in particular (2008–2012). Kilpua et al. (2014) and Selvakumaran et al. (2016) examined the interplanetary causes of low geomagnetic activity during the current SC. In more recent studies, Shanmugaraju et al. (2015) analyzed halo CMEs and their geoeffective parameters during 2011–2013 and Gopalswamy et al. (2015) discussed the MC properties during first 73 months of SCs 23 and 24 in order to ascertain the cause of the weaker geomagnetic activity during the current cycle. Shen et al. (2017) discussed the comparison of geoeffectiveness of several types of ICMEs during different solar phases for the period between 1995 and 2014. They also concluded that the probabilities of ICMEs in causing geomagnetic storms in cycle 24 are much lower compared to cycle 23.

We investigate the possible SW-IP drivers of the moderate and intense geomagnetic storms during the longest span of the current SC (24), covering ascending to early descending phases (EDPs) between December 2008 and December 2016. Therefore, our present work is the most updated study of the ongoing SC. Current study delineates the differences between the ascending to EDPs of the two consecutive SCs 23 and 24 in terms of storm occurrence distribution during both the periods, seasonal variation of storms, SW-IP conditions, and their corresponding geomagnetic response. Section 2 explains the method of determining the periods under study, the database used and selection criteria of the storm events, and identification method of their possible SW-IP drivers. Statistical results and their discussion are described in section 3, followed by the conclusion in section 4.

2. Data and Method

2.1. Sunspot Numbers

For the purpose of examining the SC variation we use SSN, which is the commonly used solar activity index. We utilize the widely used International smoothed monthly mean SSNs ($SSN_{smoothed}$), which contain the averaged over fast variations like random surges and 27-day rotational modulation. The revised version of $SSN_{smoothed}$ data is available between 1749 and May 2017 at the time of writing of this manuscript from Sunspot Index and Long-term Solar Observations (SILSO). However, after December 2016, the $SSN_{smoothed}$ data are provisional and subject to a possible revision. $SSN_{smoothed}$ value is obtained by computing a 13-month running mean of SSNs, centered at a base month and using half weights for the start and end months (Hathaway, 2010).

Figure 1 portrays the SILSO $SSN_{smoothed}$ data for the two SCs 23 and 24. It can be distinctly observed that both the cycles exhibited dual peaks. The two peaks in $SSN_{smoothed}$ for SC-23 were observed in April 2000 and November 2001 (marked by red circles), while for SC-24 were noticed in March 2012 and April 2014 (marked by blue circles).

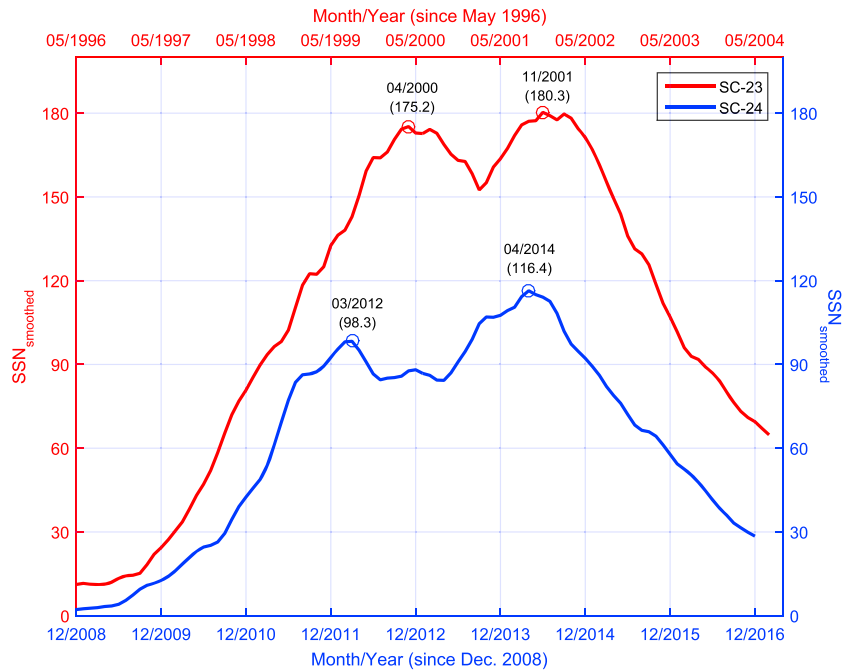


Figure 1. $SSN_{smoothed}$ from Sunspot Index and Long-term Solar Observations are plotted for ADP-23 and ADP-24 in red and blue colors, respectively. Similar color code is followed for the axes and labels related to the two curves. Upper and lower x axes refer to ADP-23 and ADP-24 respectively. The two peak values of $SSN_{smoothed}$ during ADP-23 and ADP-24 are encircled by respective colors. Corresponding time stamps for peaks are shown by adjacent text in MM/YYYY format. SSN = sunspot number; SC = solar cycle.

For the present work, we have restricted our selection of study period for SC-24 till the time when provisional *Dst* index data are available, which is December 2016. Further, for the comparison of SCs 23 and 24, we selected an interval from each cycle, which started with the respective onset of the two SCs. For the sake of inclusion of similar descending phase period from both the SCs, we chose second peak in $SSN_{smoothed}$ to be reference point. As mentioned earlier, second $SSN_{smoothed}$ peak during SC-24 occurred in April 2014; therefore, from this point to December 2016, we obtain 32-month period. Similarly, during SC-23, 32 months from November 2001 end in July 2004. In this way, the complete period of study for SC-23 is between May 1996 and July 2004 and for SC-24 is between December 2008 and December 2016. We designate the intervals including the ascending and EDPs of SCs 23 and 24, spanning between May 1996 and July 2004, and December 2008 and December 2016 as ADP-23 and ADP-24, respectively. Henceforth, this nomenclature will be used in this entire study.

We will also examine the SC variations of storms and their possible SW-IP drivers during SCs 23 and 24. For the SC phase classification, we follow the study by Gopalswamy et al. (2015), wherein the lengths of SC phases are estimated on the basis of solar polar characteristics. Arrival of polar crown filaments to $\sim 60^\circ$ solar latitudes indicate solar maximum and completion of polarity reversal at the solar poles indicate end of maximum phase. Descending phase is marked by expansion of polar coronal holes to lower solar latitudes. The periods between May 1996 and January 1999, February 1999 and June 2002, and July 2002 and July 2004 will be referred as ascending phase (AP), maximum phase (Max), and EDP for SC-23. Similarly, periods between December 2008 and August 2011, September 2011 and May 2015, and June 2015 and December 2016 will be AP, Max, and EDP for SC-24.

2.2. Geomagnetic Activity and Solar Wind Measurements

We used the *Dst* index (Sugiura, 1964), a measure of the symmetric ring current, as an indicator of geomagnetic storm intensity.

The hourly *Dst* index values are obtained from WDC, Kyoto, (<http://wdc.kugi.kyoto-u.ac.jp>). For the period between the years 1996–2014, final *Dst* index data are available and for years 2015–2016 provisional data are available. The provisional data are unverified raw data and are subjected to be adjusted after corrections.

Based on the *Dst* index, the intense geomagnetic storms are defined where minimum value of *Dst* (Dst_{\min}) ≤ -100 nT, whereas for the moderate geomagnetic storms, -100 nT $< Dst_{\min} \leq -50$ nT (Gonzalez et al., 1994).

SW-IP characteristics during the two selected intervals ADP-23 and ADP-24 are examined using hourly resolution data obtained from the OMNIWeb database (<http://omniweb.gsfc.nasa.gov/>).

3. Results and Discussion

3.1. Comparison of Two SCs

The SC-24 commenced at a very low level with a minimum SSN_{smoothed} of 2.2. On the other hand, during SC-23 the minimum SSN_{smoothed} was 11.2. The decrease between the double peaks during SC-23 and SC-24 as mentioned in section 2.1 signifies the GG identified on the basis of SSNs to be 19 months and 25 months for SC-23 and SC-24, respectively. The GG is caused by the global reorganization of solar magnetic fields (Hathaway, 2010; Storini et al., 1997, and references therein). Another striking feature is that, although for both the SCs, second peak is higher than the first one, the difference between the two peak SSN values in SC-24 is almost 3.5 times of that of SC-23. First and second peaks in the total SSNs during SC-23 and SC-24 are reflecting the peaks of sunspots in northern and southern solar hemispheres, respectively (Norton & Gallagher, 2010), which we have manually verified by the hemispherical SSN data available from SILSO (not shown here).

3.2. SC Variations of the Geomagnetic Storms

We identified a total of 196 moderate and 74 intense geomagnetic storms between May 1996 and July 2004 whereas 130 moderate and 18 intense geomagnetic storms between December 2008 and December 2016, based on the minimum *Dst* values as defined in section 2.2. It is to be pointed out that during ADP-23, among 74 intense storms, 8 were super-intense, which have minimum *Dst* ≤ -250 nT (Echer et al., 2008). In contrast, ADP-24 did not witness any super-intense event. However, in 2015, two events recorded minimum *Dst* ≤ -200 nT. Figures 2a–2d illustrate the occurrence frequency of the moderate and intense geomagnetic storms, which is defined as the total number of events/year during the two periods, ADP-23 and ADP-24, under study. SSN_{smoothed} data are shown by blue solid curves in all the panels. Figures 2a and 2b with hatched bars represent moderate geomagnetic storms, while Figures 2c and 2d with solid bars represent the intense geomagnetic storms during ADP-24 and ADP-23.

During ADP-24 (December 2008 to December 2016), out of the total geomagnetic storms, about 55% occurred during the maximum phase, among which 84% are moderate and the remaining 16% are intense. In contrast, the ascending phase witnessed only moderate storms, while the EDP evidenced 35% of total storms during ADP-24, out of which $\sim 90\%$ are moderate. Hence, it is distinctly noticeable that the entire ADP-24 period is dominated by moderate storms.

During ADP-24, moderate geomagnetic storms show a steady increase in occurrence frequency in concurrence with the SSNs from 2009 to 2013 as shown in Figure 2a. There were no moderate storms in December 2008. Toward the end of 2008 and 2009, the low-latitude coronal holes disappeared, and hence, no sources of HSS existed, which explains the reduction of moderate geomagnetic storms in 2009 as compared to the period between January 2008 and November 2008 (not shown; De Toma, 2011; Gibson et al., 2009; Tsurutani et al., 2011). In addition, Tsurutani et al. (2011) ascertained the low geomagnetic activity during 2009 to be contributed by the predominance of slow solar wind streams and abnormally low IMF strength. Another noteworthy point seen in Figure 2a is that ADP-24 witnessed increased occurrences of moderate storms during GG, compared to that around first SSN_{smoothed} maximum.

Figure 2b indicates that the moderate geomagnetic storms occurrence during ADP-23 also follows the increasing trend of SSNs between 1996–2000. Noteworthy point is the reduction observed in the number of moderate geomagnetic storms around the second peak of ADP-23 and ADP-24. As previously remarked, the total number of moderate storms during ADP-23 and ADP-24 is 196 and 130, respectively. Occurrence rates of moderate geomagnetic storms during ADP-23 and ADP-24 are 23.8 storms per year and 16.1 storms per year, respectively.

Figure 2c clearly indicates that during the first 2 years of the cycle 24 there were no intense geomagnetic storms recorded. Only in the subsequent years, the intense geomagnetic storm occurrence commenced. The rate of occurrence of intense geomagnetic storms during ADP-24 is 2.2 storms per year. For the SC-24, the first peak of the sunspots cycle (Northern Hemisphere) occurred in 2012, and concurrently, the intense storm occurrence also exhibited a peak in 2012 (Figure 2c). An interesting observation is that around the time

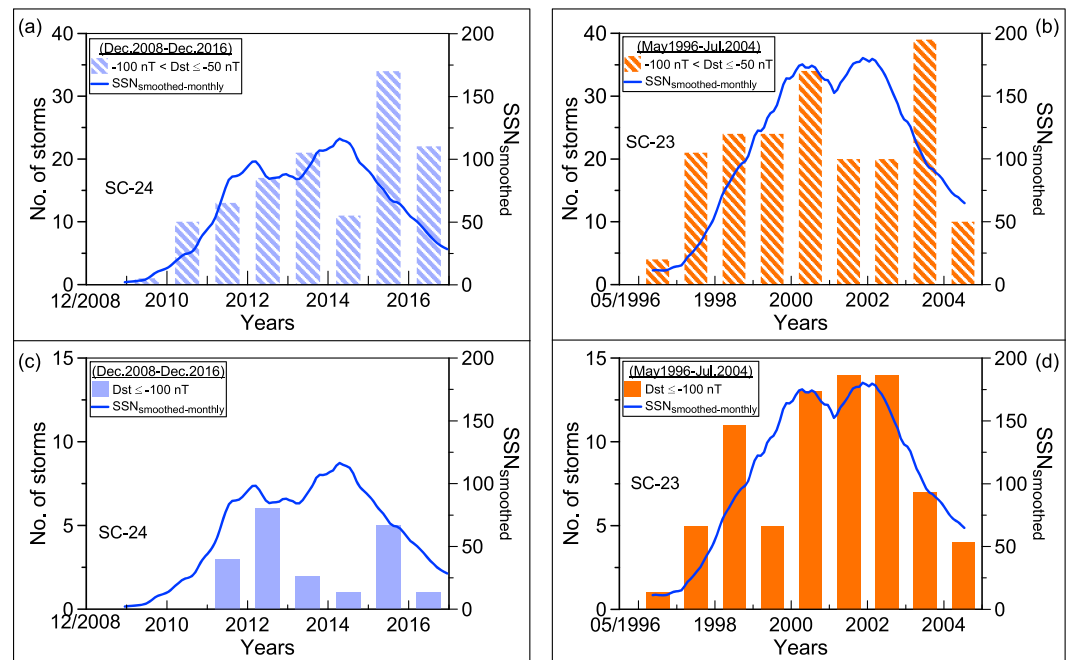


Figure 2. Solar cycle distribution of geomagnetic storms occurred during ADP-23 and ADP-24. Hatched bars in top panels (a) and (b) display moderate storms, and solid bars in bottom panels (c) and (d) demonstrate intense storms. Blue color represents ADP-24, and orange color represents ADP-23. Blue solid curves in panels (a)–(d) indicate $SSN_{smoothed}$ for both the cycles. SC = solar cycle; SSN = sunspot number.

of the second (southern hemispheric) sunspot peak, the intense storm rate did not increase. This may be associated with the great active region (AR) 12192, which harbored large sunspot group and was prolific flare producer (Chen et al., 2015; Sun et al., 2015). Although (AR) 12192 produced series of solar flares during October 2014 but almost all were without CME association, known as confined flares. Absence of CMEs and their ICMEs clearly supports the abrupt reduction in the geomagnetic activity during 2014. On the other hand, for SC-23, both the sunspot maxima witnessed almost comparable number of intense geomagnetic storms as can be seen from Figure 2d, which delineates the yearly occurrence frequency of the intense geomagnetic storms during ADP-23. It is clearly seen that ADP-23 witnessed intense geomagnetic storms right from the SC commencement (1996). The intense storm occurrence rate during ADP-23 is ~ 9 storms per year. Thus, ADP-23 exhibited a striking enhancement in the rate of intense storms by a factor of ~ 4 as compared to that during ADP-24. The noticeable reduction in the number of intense geomagnetic storms during 1999 is attributed to the decreased number of ICMEs (Cane & Richardson, 2003).

Table 1 displays the storm comparison for the two selected periods ADP-23 and ADP-24. During each period, ADP-23 and ADP-24, we calculated the average of absolute Dst_{min} value ($\langle |Dst_{min}| \rangle$) obtained during all the storms ($Dst \leq -50$ nT) and we found that $\langle |Dst_{min}| \rangle$ during ADP-23 is only about 23% higher than during ADP-24. We also calculated the range of Dst_{min} for all the storms. We define this range as the difference between -50 nT and the lowest Dst_{min} values obtained among total 270 and 148 storms occurred

Table 1
Comparison of All the Storms With $Dst \leq -50$ nT Occurred During ADP-23 and ADP-24

SC period	Total storms	Moderate storms (-100 nT $< Dst \leq -50$ nT)	Intense storms ($Dst \leq -100$ nT)	Superstorms ($Dst \leq -250$ nT)	$\langle Dst_{min} \rangle$	Dst_{min} range
ADP-23	270	196	66	8	-91.4	372
ADP-24	148	130	18	0	-74.2	173

Note. Column 1 represents the solar cycle phases for the two cycles. Columns 2–5 indicate number of storms falling in the specified category. In this table, super-storm subset has been extracted from total intense storms ($Dst \leq -100$ nT) itself. Column 6 gives the average of Dst_{min} (nT) value of all the storms during each period (ADP-23 and ADP-24). Column 7 indicates the Dst_{min} (nT) range defined as the difference between highest and lowest Dst_{min} (nT) values among all the storms of ADP-23 and ADP-24.

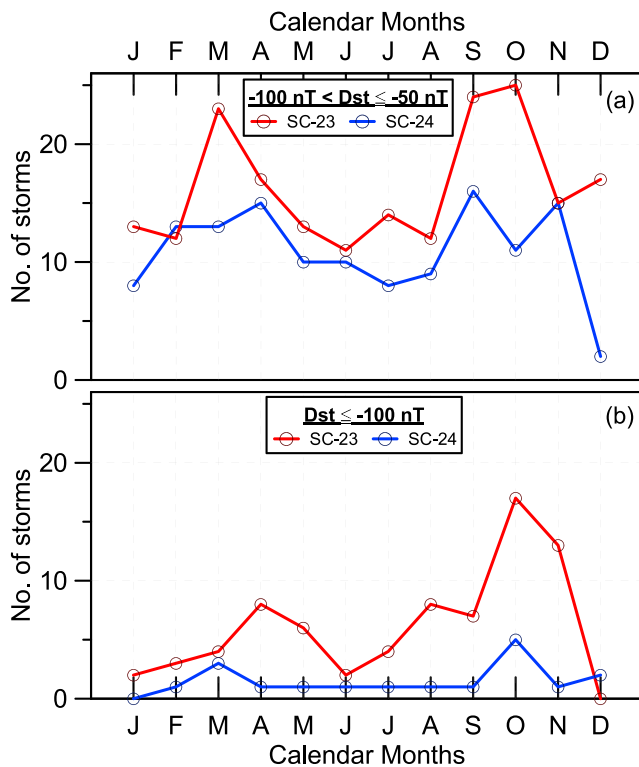


Figure 3. Seasonal distribution of the (a) moderate storms ($-100 \text{ nT} < Dst_{\min} \leq -50 \text{ nT}$) and (b) intense storms ($Dst_{\min} \leq -100 \text{ nT}$) between January (J) to December (D) calendar months during ADP-23 and ADP-24. SC = solar cycle.

and dipole axis; the maxima of geomagnetic activity occur when the geomagnetic dipole axis is perpendicular to the Sun-Earth line. RM hypothesis explains the semiannual variation in terms of variation of the angle between the IMF B_z and that of the Earth's magnetic dipole axis. Accordingly, the geomagnetic activity is maximum when IMF B_z is minimum in the solar magnetospheric coordinate system, which occurs near equinoxes Zhao and Zong (2012). Another study on the seasonal variation of geomagnetic activity was carried out by Mursula et al. (2011) and Zieger and Mursula (1998), concluding that geomagnetic activity exhibits equinoctial maxima, which alternates between vernal and autumnal equinoxes during even and odd SCs, respectively.

Figure 3 illustrates the seasonal variation in the occurrence of moderate (Figure 3a) and intense (Figure 3b) geomagnetic storms per calendar month during ADP-23 and ADP-24. The seasons here are considered as in the Northern Hemisphere. It is observed that both the cycles distinctly exhibit the well-known semiannual variation in both the moderate and intense storm rates, with two peaks, one around vernal (February to April) equinox and another around autumnal (August to October) equinox (Cortie, 1912; Echer et al., 2011; Priestler & Catanni, 1962; Russell & McPherron, 1973). We would like to mention that though the number of intense storms is too small for robust seasonal variation statistics, at least the behavior is consistent with the expectation. Consistent prevalence of higher seasonal storm activity during ADP-23 as compared to ADP-24 is noteworthy.

For the moderate storms, the autumnal equinox peaks are larger than the vernal equinox in cycle 23 (Figure 3a) but not in cycle 24 (so far as statistics allow a comparison). Thus, cycle 23 is consistent with Zieger and Mursula (1998) and Mursula et al. (2011), but cycle 24 may not be.

For the intense geomagnetic storms it is noticeable that during ADP-24 both the equinoxes witnessed almost comparable number of storms. However, it is to be pointed out that since the number of intense storms is small during ADP-24, no conclusive comment on their seasonal asymmetry can be made (Figure 3b). In contrast, during ADP-23, the intense storm seasonal statistics clearly exhibits the vernal-autumnal equinoctial

during ADP-23 and ADP-24, respectively. For ADP-23 storms, Dst_{\min} range is 372 nT, while for ADP-24 storms it is 173 nT. We obtained that Dst_{\min} range for ADP-23 is almost twice than that of ADP-24, which distinctly reflects the extremity of geomagnetic activity during ADP-23. Gonzalez et al. (1990) and Echer et al. (2011, 2013) have studied the SC distribution of geomagnetic storms during several cycles and obtained that geomagnetic storm occurrence exhibits a dual peak, with one peak occurring in late ascending or maximum phase and another peak in EDP. We obtained that ADP-24 clearly follows the dual peak characteristic in the moderate (Echer et al., 2013) and intense storm occurrence rates as distinctly observed from Figures 2a and 2c. One of the peaks in the moderate storm rate occurred around maximum phase (2013) and another peak around EDP (2015). Similar observation is obtained for the intense storm rate, for which first peak occurred around maximum phase (2012) and a second peak is observed during (2015).

3.3. Seasonal Variations of Storms

The characteristic feature of two peaks in the geomagnetic activity around equinoctial months has been well studied since past several decades using various geomagnetic indices like aa , Ap , Dst , and AE (e.g., Ahn et al., 2000; Chapman & Bartels, 1940; Cliver et al., 2000; Cortie, 1912; Lyatsky et al., 2001; Oh & Yi, 2011; Russell & McPherron, 1973). The main possible mechanisms to explain the semiannual variation of geomagnetic activity include axial model (Cortie, 1912), equinoctial model (Chapman & Bartels, 1940), Russell-McPherron (RM) model (Russell & McPherron, 1973), and the solar illumination hypothesis (Lyatsky et al., 2001). The axial model accounts for 7.2° tilt of solar rotation axis with respect to the ecliptic plane. The equinoctial hypothesis is based on the 23° tilt of the Earth's equatorial plane to the ecliptic plane and 11° offset between the Earth's rotation

asymmetry as discussed by Zieger and Mursula (1998); Mursula et al. (2011). Hence, our results for intense storms of SC-23 (odd cycle) are in conformity with the previous studies by Zieger and Mursula (1998) and Mursula et al. (2011), but the SC-24 intense storms do not conform with them.

Currently, we have considered only the two SCs; hence, above results will be tested on the other SCs for robustness in the future work.

3.4. Comparing the Solar Wind Plasma and IMF Conditions in Cycles 23 and 24

Comparison of the two consecutive SCs would not be complete without examining the long-term variation of solar wind plasma and IMF parameters with the SSNs.

For this purpose, continuous hourly resolution solar wind and IMF data from OMNIWeb database is utilized during May 1996 to July 2004 and December 2008 to December 2016 intervals. We applied cumulative probability distribution function (CDF) to delineate the comparison between the occurrence probabilities of different values of the important parameters that majorly contributed to the geomagnetic storm activity during ADP-23 and ADP-24. The significance of applying CDF rather than using discrete yearly averages is that it projects the prevalent differences between the two cycles in a remarkably distinguishable manner.

To obtain the CDF plots, we followed these steps:

- i. Sort the solar wind, IMF, and geomagnetic observations, viz., V_{sw} , E_y , B_s , and Dst , for both the periods ADP-23 and ADP-24 separately in ascending order of values.
- ii. Find the probability of occurrence of \leq (\geq) each observation (" k ") of individual negative (positive) parameter (" t ") in the sorted array
- iii. If " n " is the total number of samples, then the empirical cumulative distribution function (ecdf) is defined as a step function (F) that has a step of k/n . The subsequent observations are cumulative sum of previous observations.
- iv. Plot sorted observations of individual parameter (t) and obtained probabilities (step function, F).

Figures 4a–4d exhibit the CDF curves for solar wind speed (V_{sw}), B_s ($| -B_z |$), duskward (positive) E_y (E_{dusk}), and Dst . Red and blue curves in Figure 4 represent ADP-23 and ADP-24, respectively. Figure 4a depicts the CDF plot for the solar wind speed where it is distinctly observed that the probability of observing higher-speed solar wind is consistently higher for ADP-23 (red) than for ADP-24 (blue). The peak V_{sw} values as found in OMNIWeb data base during ADP-23 and ADP-24 are 1,183 and 904 km/s, respectively.

From Figure 4b it is clearly observed that the probability of exceeding the lower B_s values is almost comparable for ADP-23 and ADP-24; however, the probability of exceeding the higher B_s values goes on decreasing for ADP-24. The lowest value of hourly B_s during ADP-23 is 50.9 nT, which is almost double of that during ADP-24 (~ 24.1 nT; Figure 4b).

Figure 4c distinctly shows that similar CDF profiles are obtained for E_{dusk} values for both the periods. From Figure 4c, we obtain the highest value of E_{dusk} for ADP-23 is 35.3 mV/m, which is almost 2 times of that of highest E_{dusk} value during ADP-24 (16.09 mV/m).

The geomagnetic response of varying interplanetary conditions during ADP-23 and ADP-24 is represented by Dst in Figure 4d. The lowest values of Dst during ADP-23 and ADP-24 are -422 and -223 nT, respectively. It is noticeable from Figure 4d that the Dst CDF profiles for the two periods start to diverge from the smallest negative Dst values.

We attempted to check the occurrences of -100 nT $< Dst \leq -50$ nT values representing moderate geomagnetic activity and $Dst \leq -100$ nT representing intense activity during the two periods (ADP-23 and ADP-24). We obtained that the occurrence of moderate geomagnetic activity in ADP-23 is ~ 2.4 times of that in ADP-24, in contrast to the occurrence of intense activity which is >6 times of the latter (ADP-24).

Interplanetary causes of intense geomagnetic storms are long-duration (>3 hr), large B_s (>10 nT), associated with $E_{dusk} > 5$ mV/m (Gonzalez & Tsurutani, 1987). For the moderate storms, Gonzalez et al. (1994), Wang et al. (2003), and Echer et al. (2013) suggested the interplanetary criteria of $B_s > 5$ nT associated with $E_{dusk} \geq 2.5$ mV/m for >2 hr. Rawat et al. (2010) analyzed big storms ($Dst \leq -200$ nT) during SC 23 and concluded the interplanetary conditions for them to be $B_s \geq 20$ nT with $E_{dusk} > 12$ mV/m. With these criteria, we determined the occurrences of geoeffective B_s and E_{dusk} , contributing to the moderate, intense, and super-intense/extreme geomagnetic storms. For this, we applied three threshold cutoffs (5, 10, and 15 nT)

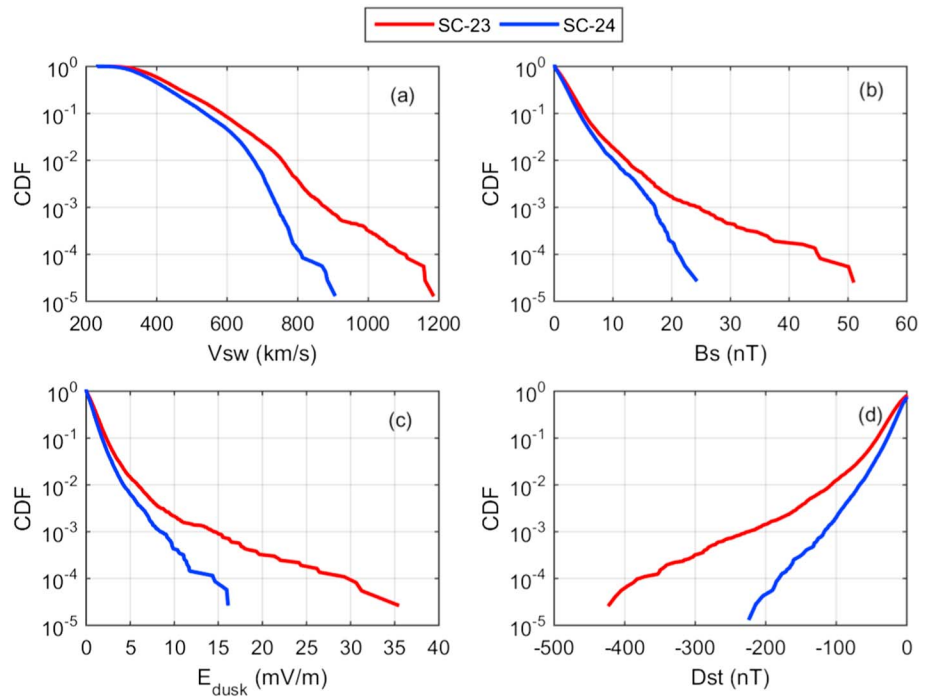


Figure 4. Cumulative probability distribution of solar wind-interplanetary and geomagnetic parameters including (a) V_{sw} , (b) B_s ($| -B_z |$), (c) E_{dusk} , and (d) Dst during the ascending to early descending phases of solar cycles 23 and 24. The cumulative probability is computed using continuous hourly solar wind, interplanetary magnetic field, and Dst data for ADP-23 and ADP-24. For positive quantities (V_{sw} , B_s , and E_{dusk}) the ordinate is the probability of exceeding the abscissa. On the other hand, for the negative quantity (Dst), the ordinate is the probability of being less than the abscissa. SC = solar cycle; CDF = cumulative distribution function.

to B_s values and three threshold cutoffs on the values of $E_{dusk} \geq 2.5$, ≥ 5 , and ≥ 12 mV/m during both the periods, ADP-23 and ADP-24. The occurrence of B_s and E_y values fitting to the threshold criteria as discussed above during ADP-23 and ADP-24 is represented in tabular format (Table 2).

The study by Gonzalez et al. (2011) on super-intense and extreme ($Dst < -400$ nT) geomagnetic storms occurred during cycle 23 affirmed that the average peak B_s value for super-intense storms is 34.3 nT with average peak E_{dusk} value of 23.5 mV/m. During ADP-24, the absence of super-intense storm/superstorm ($Dst \leq -250$ nT) could be attributed to the insignificant values of minimum essential thresholds of geoeffective SW-IP parameters, B_s and E_{dusk} in this period.

3.5. Long-Term SC Variability

The main objective of our present study is to compare the two SCs in terms of SW-IP conditions and their corresponding geomagnetic activity. In the above subsections, we have demonstrated the distinction between specific characteristics of the conditions during both the selected periods.

In order to compare the solar wind conditions during both cycles in correspondence with the variations in smoothed SSNs (13 month averaged), we computed 13-month smoothed values of B_z , B_{tot} , V_{sw} , and E_y . Sunspot cycle variation of 13-month averaged Dst values is also shown. We obtained the daily data values from the Omniweb database and averaged them to get monthly values. The smoothing

of all the parameters is performed exactly in the way done for sunspot smoothing given in section 2.1 (Hathaway, 2010). It should be noted that such smoothing provides information on the average parameters. The results for ADP-23 (red) and ADP-24 (blue) are illustrated in Figures 5a–5f. It is to be mentioned that the time axis for ADP-23 is plotted on the top (red) and for ADP-24 is plotted at the bottom (blue). First striking difference observed between the two intervals is that ADP-23 is stronger in terms of B_{tot} , southward directed B_z , solar wind speed, electric field, and corresponding geomagnetic response represented by Dst index.

Table 2
Percentage of Occurrence of Geoeffective Solar Wind-Interplanetary Parameters for Different Threshold Values During the Two Periods

Parameter	Period	% (Threshold values)		
B_s (nT)	ADP-23	10.5%(5)	1.9%(10)	0.17%(20)
	ADP-24	7.1%(5)	1%(10)	0.02%(20)
E_{dusk} (mV/m)	ADP-23	7.9%(2.5)	1.4%(5)	0.14%(12)
	ADP-24	4.4%(2.5)	0.6%(5)	0.01%(12)

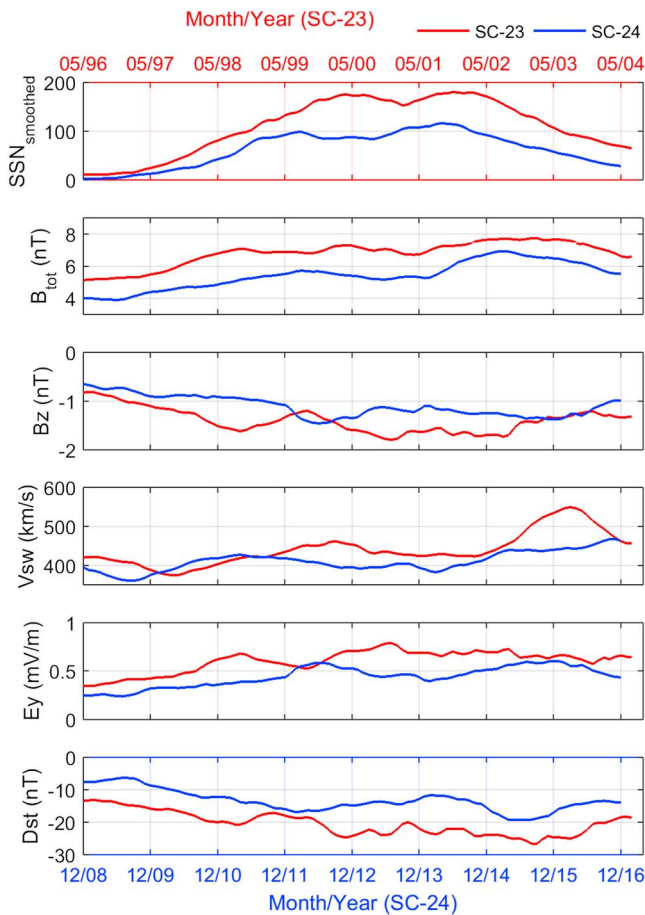


Figure 5. Variation of solar wind, interplanetary, and geomagnetic parameters in correspondence with the smoothed sunspot numbers for ADP-23 red and ADP-24 blue. From top to bottom, the panels depict (a) $SSN_{smoothed}$, (b) B_{tot} , (c) B_z , (d) V_{sw} , (e) E_y , and (f) Dst . The solar wind-interplanetary parameters and Dst index are smoothed using 13-month running average. The top red and bottom blue x axes display the months in month/year format for SC-23 and SC-24, respectively. The first values of both the x axes mark the solar minimum months for SC-23 and SC-24, which are May 1996 and December 2008, respectively.

B_{tot} exhibits a steadily increasing profile during the ascending phases of both the cycles, which is consistent with the well-known SC variation in the IMF strength (Gazis, 1996). However, B_{tot} in SC-23 is always higher than in SC-24 as seen in Figure 5b. Further, B_{tot} appears to be enhanced following the solar maximum into the EDPs of both the cycles as also discussed by Wang and Sheeley (2015) and Sheeley and Wang (2015) in their studies of sources of SC variation of the IMF. They explained this *rejuvenation* in the field to be caused by the emergence of large active regions with their east-west dipole moments arranged in phase with the Sun's dipole moment (background field), thereby resulting in strengthening of the same.

During ADP-23, B_z (red curve in Figure 5c) exhibits three periods of depressions, one around late ascending phase to early maximum phase (January 1998 to September 1999) and second and third deeper ones during the maximum phase (2000–2002). Similarly, during ADP-24 (blue curve) we observe that a steady depression in B_z values continued until 2012, where first B_z minimum is seen (Figure 5c). This is nearly coincident with the onset of maximum phase of the SC-24, as seen in Figure 5a. The B_z depression trend during ADP-24 was followed by a slight recovery during maximum phase (2012–2013) and a further weaker depression while sunspot cycle progressed toward the declining phase, post 2014. A weaker average B_z is noticeable between the two minima (Figure 5a) during ADP-23 and ADP-24. During the GG, the period of almost steady weaker $SSN_{smoothed}$ in ADP-24 was distinctly marked by increase in B_z values.

It is to be pointed out that heavy averaging (13-month running basis) of the SW-IP data has resulted in much smaller values of parameters in comparison to the original daily resolution data as seen in Figures 5a–5f; nevertheless, the similarity in the SC variation pattern of the SW-IP parameters during two different SCs 23 and 24 is clearly reflected.

Referring to ADP-23 (red curve) in Figure 5c and occurrence rate of intense storms Figure 2d, it can be clearly seen that ADP-23 intense storm rates correspond well to the stronger southward B_z around 1998 and 2000–2001. Similarly, Figures 5c and 2c suggest existence of reasonable concurrence between stronger southward B_z values around 2012 and 2015 during ADP-24 and the enhanced intense storm rates in these years.

We are looking at the long-term variations in both the cycles, and this result shows that the average stronger B_z are observed in cycle 23 and that might have resulted in larger geomagnetic activity in comparison to cycle 24, as seen in the averaged geomagnetic activity represented by Dst in Figure 5f. Predominance of slow solar wind streams and abnormally low IMF strength during the deep solar minimum between the cycles 23 and 24 led to very low energy transfer from solar wind to the magnetosphere, and the geomagnetic activity reached extremely low levels (Echer et al., 2012; Tsurutani et al., 2011). From Figure 5d), distinct V_{sw} depression is seen around the solar minima/ascending phases of SC-23 and SC-24, which signifies the shrinking and poleward migration of the high-latitude coronal holes after the declining phase of the previous cycle as explained by McComas et al. (2000). With the emergence of sporadic low-latitude coronal holes during the commencement of new cycle the solar wind speeds exhibit enhancement. During the period between 1999 and 2000 in ADP-23, peak in V_{sw} indicates presence of HSS, as reported by Echer et al. (2013) and Hajra et al. (2013). Bothmer and Zhukov (2007) discussed the decrease in number of CMEs during the year 1999 in terms of enhanced fast solar wind flows and CIRs. Declining phases of both the SCs witnessed enhancements in V_{sw} , which might have contributed to the increased occurrences of moderate storms.

Figure 5e shows the convection electric field (E_y) time variation in reference to the SSNs. It is observed that during ADP-23, E_y exhibits triple peak feature in concurrence with the three B_z minima. The first peak of E_y around

Table 3
Complex and Uncertain Category of Geomagnetic Storm Events With $Dst_{min} \leq -50$ nT Between the Period December 2008 and December 2016

Date	Dst_{min}	Category
15/2/2010	-59	Complex
5/7/2011	-59	Uncertain
12/6/2012	-51	Uncertain
4/9/2012	-63	Complex
24/4/2013	-50	Complex
7/11/2013	-54	Uncertain
20/1/2016	-93	Complex
31/1/2016	-50	Complex
3/2/2016	-52	Complex
2/4/2016	-56	Complex
7/4/2016	-60	Complex
16/4/2016	-55	Complex
08/5/2016	-83	Complex

Note. Date is formatted as date/month/year.

1998 (ascending phase) is smaller than the second and third peaks around SC maximum. The occurrences of three peaks in E_y values during ADP-23 are nearly coincidental with enhancements in intense storm occurrences around 1998 and solar maximum during ADP-23 (refer to Figure 2d). Similar observation is obtained for ADP-24, where peak in E_y during 2012 is almost concurrent to the enhanced occurrence of intense geomagnetic storms (Figure 2c). Also, another rise in E_y around 2015 is distinctly evident from Figure 5e, which again is nearly coincident with the intense storm occurrence in 2015. Reduction in E_y during GG is clearly observed in both the curves of Figure 5e.

The fact that the solar wind-magnetosphere coupling was weaker in cycle 24 than in cycle 23 is due to a less active Sun. The lower solar magnetic field (Tsurutani et al., 2011) and the lower number of solar eruptions (Gopalswamy et al., 2015) lead to a smaller number of transient geoeffective solar wind structures and thus in a much reduced number of intense storms.

3.6. Geoeffective SW-IP Drivers Over Cycle 24

Several studies have been done on the identification of potential SW-IP origins of the geomagnetic storms and differentiation between them (Borovsky & Denton, 2006; Huttunen et al., 2002; Saiz et al., 2013; Tsurutani & Gonzalez, 1997; Zhang et al., 2007). Mostly, studies are consistent with the

dominance of ICMEs and/or their sheaths during the rising and maximum phases of the SCs (e.g., Echer et al., 2008; Gonzalez et al., 1999; Richardson, 2013; Tsurutani et al., 1988; Zhang et al., 2007).

In the present work, the SW-IP driver for each event has been identified by careful examination of the solar wind plasma and magnetic field characteristics. We classify the drivers into six categories, adapting the nomenclature of Echer et al. (2008); namely,

SH - pure sheath

MC - interplanetary coronal mass ejections exhibiting magnetic cloud structures

SH+MC - combination of sheath and magnetic cloud (SH+MC)

CIR - corotating interaction region

ICME - interplanetary coronal mass ejections which do not have any identifiable magnetic cloud structure (non magnetic cloud ICME)

SH+ICME - sheath followed by ICME (non magnetic cloud ICME).

In addition, we found some different kind of events, which were designated as *Complex*. These include the heliospheric plasma sheet or heliospheric current sheet/sector boundary crossing interacting with SH/ICME, CIR following a SH or MC, interaction of sector boundary crossing with CIR. There were three events for which the interplanetary structure were not identifiable and hence have been put under *Uncertain* category (Table 3).

The SW-IP drivers causing the intense geomagnetic storms during ADP-24 are laid down in Table 4. Columns 1 to 5 in Table 4, respectively, depict the storm day when minimum Dst was recorded, peak B_s , value of Dst_{min} , and causative SW-IP driver.

In addition, we also present the yearly distribution of the SW-IP drivers causing moderate and intense geomagnetic storms occurred during ADP-24 in Table 5. Column 1 indicates years between December 2008 to December 2016; columns 2 to 5 represent the four major SW-IP drivers, namely, SH, ICME, SH+ICME, and CIR. Last two columns indicate complex or uncertain SW-IP structures as described above in classification. In this table we put all the drivers exhibiting ICME signatures like MCs, non-MCs, slow ICME, shock/MC, and shock/ICME under same class, ICME.

During the complete ADP-24 period, the major drivers for most of the moderate storms were CIRs (~41%) followed by ICME (20%), SH+ICME (15.4%), and SH (13.8%). Echer et al. (2013) studied the moderate storms during the complete SC 23. Their statistics showed that the moderate storms during cycle 23 were caused majorly by CIRs 48%, while ICMEs (MCs or non-MC ICMEs), SH fields, and combination of SH and ICME accounted for 20.6%, 10.8%, and 9.9%, respectively.

Table 4
SW-IP Drivers Causing the Intense Geomagnetic Storm Events
($Dst_{min} \leq -100$ nT) During ADP-24 (December 2008 to December 2016)

Date	B_{speak} (nT)	Dst_{min} (nT)	SW-IP structure
6/8/2011	19.3	-115	SH
26/9/2011	24.1	-118	SH
25/10/2011	13.1	-147	SH+MC
9/3/2012	16.4	-131	SH+ICME
24/4/2012	10.8	-108	SH+MC
15/7/2012	17.3	-127	MC
1/10/2012	19.2	-119	MC
9/10/2012	14.1	-104	MC
14/11/2012	17.2	-108	MC
17/3/2013	11.5	-132	SH+MC
31/5/2013	16.2	-119	CIR
19/2/2014	12.9	-116	MC
17/3/2015	17.3	-223	SH+ICME
23/6/2015	22.2	-204	SH
7/10/2015	8.5	-124	CIR
20/12/2015	17.9	-155	SH+ICME
31/12/2015	15.8	-110	SH+MC
13/10/2016	20.8	-104	SH+MC

Note. Date is formatted as date/month/year. SW-IP = solar wind-interplanetary; MC = magnetic cloud; ICME = interplanetary coronal mass ejection; CIR = corotating interaction region.

Figure 6 illustrates the SC distribution of SW-IP drivers causing the moderate and intense geomagnetic storms during ADP-24 (Figures 6a and 6b, respectively). First, we consider only the moderate geomagnetic storms as depicted in Figure 6a. The ascending phase is predominated by the CIR-driven geomagnetic storms (50%), whereas the maximum phase is dominated by pure SH, ICME, CIR, and SH+ICME-driven geomagnetic storms. The contribution from ICMEs and/or their SH in Max was almost 66%. EDP was again marked by dominance of CIR-driven storms (56%) over ICMEs and/or their SH. ICME and/or their SH contributed for about 33% of the moderate storms in EDP.

Echer et al. (2013) performed the SC distribution analysis of the moderate storms occurred during the SC 23 and concluded that CIRs are responsible for almost 60% of the moderate storms during the declining phase of cycle 23, also CIRs accounted for 30–35% storms during rising and maximum phases of SC-23. ICMEs and/or their SH stood out as major drivers (51–54%) during the ascending and maximum phases. Hence, our results are in close agreement with Echer et al. (2013) results. Both the SCs (23 and 24) are similar in terms of the SW-IP drivers of moderate storms.

We now consider the SC variability of the drivers for the intense storms during ADP-24, as shown in Figure 6b. During the ascending phase of SC-24 (December 2008 to August 2011), only one intense storm occurred on 5 August 2011, which was driven by sheath (SH). In contrast, the maximum phase (September 2011 to May 2015) evidenced 12 intense geomagnetic storms. Noticeable point is that for all the 12 intense storms a distinct dominance of ICME (42%) followed by SH+ICME 33% and pure SH 17% was exhibited. Our investigation showed that all the ICMEs contributing for the intense storms during maximum phase of SC-24 were ICMEs exhibiting MC signatures; hence, MC contributed about 42% for the intense storms. There was only one intense geomagnetic storm caused by CIR during the maximum phase.

In the EDP (June 2015 to December 2016), only five intense storms were recorded and for them SH+ICME majorly (60%) contributed toward the intense storms. Among the total three SH+ICME storms, there was only one intense storm driven by SH+MC, other two were SH+ICME (non-MC). In this phase, out of the remaining two intense storms, one of which was driven by SH and the other by CIR and thereby each contributed about

Table 5
Yearly Distribution of the SW-IP Drivers Causing All the Geomagnetic Storm Events
($Dst_{min} \leq -50$ nT) Between the Period December 2008 and December 2016

Year	SH	ICME	SH+ICME	CIR	Complex	Uncertain
December 2008	—	—	—	—	—	—
2009	—	—	—	1	—	—
2010	1	1	3	4	1	—
2011	7	2	2	4	—	1
2012	3	9	6	3	1	1
2013	6	3	5	7	1	—
2014	2	6	3	1	—	—
2015	3	7	7	22	—	—
2016	—	3	1	13	7	1
Total	22	31	27	55	10	3

Note. Here we have considered all the ICME structures irrespective of showing the MC or non-MC characteristics. SW-IP = solar wind-interplanetary; ICME = interplanetary coronal mass ejection; CIR = corotating interaction region; MC = magnetic cloud.

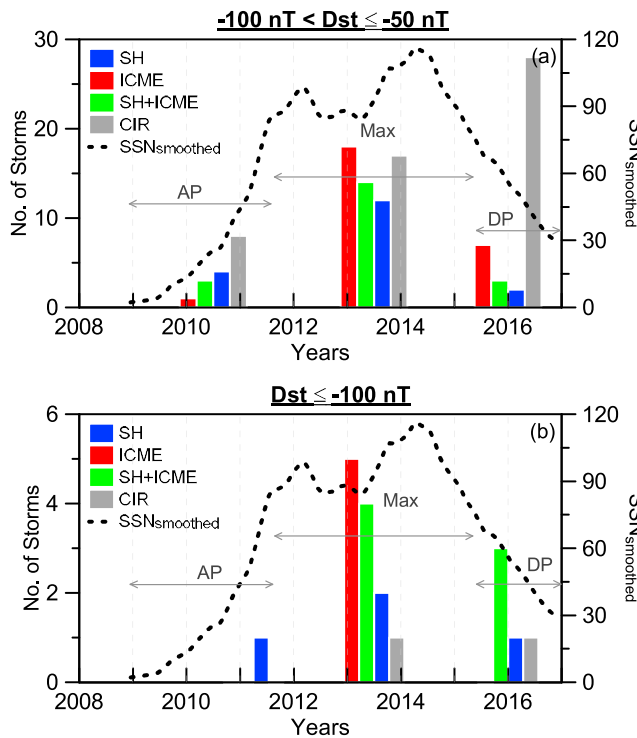


Figure 6. Solar cycle distribution of solar wind-interplanetary drivers causing geomagnetic storms during ascending (December 2008 to March 2011), maximum (April 2011 to May 2015) and early descending phases (June 2015 to December 2016) of the solar cycle 24. Labels AP, Max, and EDP indicate ascending phase, maximum, and early descending phase, respectively for (a) moderate geomagnetic storms and (b) intense geomagnetic storms. Red, blue and green bars represent ICME, SH and SH+ICME respectively. Gray bars depict CIRs. Black dashed curve represent $SSN_{smoothed}$. ICME = interplanetary coronal mass ejection; CIR = corotating interaction region; DP = descending phase.

20% in declining phase. Echer et al. (2013) also concluded that CIRs caused up to $\sim 20\%$ of the intense storms in the declining phases of cycle 23.

Gonzalez et al. (2007) and Echer et al. (2008) examined SW-IP drivers responsible for the intense storms during SC 23. They showed that MCs are primary drivers for the intense geomagnetic storms during rising and declining phases of SC-23, while sheath dominates the solar maximum. Shen et al. (2017) study shows that large fraction (75%) of the geomagnetic storms (moderate and intense) during 1995–2015 are caused by the ICME groups and almost all the intense geomagnetic storms during the period were caused by ICMEs.

Our SW-IP drivers discussion implies that during ADP-24, either the geoeffective SW-IP structures like ICMEs and/or their sheaths were reduced in number substantially or they did not possess significantly large southward directed B_z , in comparison to that during ADP-23. Previous work by Richardson (2013) concludes that an absence of large southward B_z in SH/ICMEs and low speeds of ICMEs contributed to the reduced geoeffectiveness of SH/ICMEs in the rising phase of SC-24 (December 2008 to November 2012) compared to that of SC-23. Kilpua et al. (2014) examined the causes for geomagnetic storms to be weak during the recent solar minimum and rising phase of cycle 24. They ascertained the primary reason to be the lack of strong and long-duration ICMEs with southward IMF. Hence, our findings are in close agreement with Richardson (2013) and Kilpua et al. (2014). Similar conclusions were reached by Gopalswamy et al. (2015) in their recent study involving the comparison of MCs during the SCs 23 and 24. Another interesting study was done by Shanmugaraju et al. (2015), wherein they discuss the physical characteristics of halo CMEs occurred during 2011–2013 and their geoeffective parameters. The much weaker geoeffectiveness in the rising phase of SC 24 than that in cycle 23 was evident in their study as well.

Having demonstrated the SC distribution of various SW-IP drivers, we further compared the sizes of the geoeffective solar wind parameters in

individual storm drivers. In order to do so, we performed correlation analysis between the solar wind plasma and magnetic field parameters (E_y , B_z , and V_{sw}) and Dst index for all the storms caused by the four major SW-IP drivers: (1) ICME (including MC and non-MC), (2) SH, (3) SH+ICME (including SH+MC), and (4) CIR during December 2008 to December 2016. For the correlation analysis, we considered hourly values of Dst_{min} , peak E_y ($E_{y_{peak}}$), $B_{z_{min}}$, and $V_{sw_{peak}}$ for the individual events for all the major drivers.

Gonzalez et al. (2007) proposed that a time lag ranging from 0 to 4 hr exist between minimum B_z and Dst_{min} , which is described as the response time of geomagnetic field to IMF B_z conditions. Considering this, we kept a search window of 0–4 hr for selecting the $B_{z_{min}}$ and $E_{y_{peak}}$ after obtaining the time of minimum Dst (Dst_{min}). Although we recognize that the Dst index is driven by the time integral of E_y (Burton et al., 1975), here we use the peak values in the search window to make a simple comparison between drivers.

Earlier studies on geoeffective SW-IP structures by Echer et al. (2008, 2013) and Richardson (2013) have presented the correlations between peak values of several SW-IP parameters, but those show collective results for ICMEs, their sheaths, etc. Our work, however, presents individual correlations for the four major SW-IP drivers including ICME (MC and non-MC), SH, SH+ICME (and SH+MC), and CIR. We compare the correlations between the vital solar wind plasma and IMF parameters in the major SW-IP drivers of storms occurred during ADP-23 and ADP-24, causing the storms with $Dst_{min} \leq -50$ nT and the Dst index itself (Figures 7 and 8). It is to be mentioned that top three panels in each box are for ADP-23, while lower three panels are for ADP-24. Figures 7a–7f represent the correlations of $E_{y_{peak}}$, $B_{z_{min}}$, and $V_{sw_{peak}}$ with Dst_{min} for storms driven by MCs and non-MC-ICMEs. The linear fits for two classes are shown by solid and dashed lines, respectively. Figures 7g–7l illustrate the correlations for pure SH. Correlation for storm events driven by interacting SH+ICME (MC and non-MC) and CIR have been depicted in two boxes of Figures 8a–8f and 8g–8l, respectively.

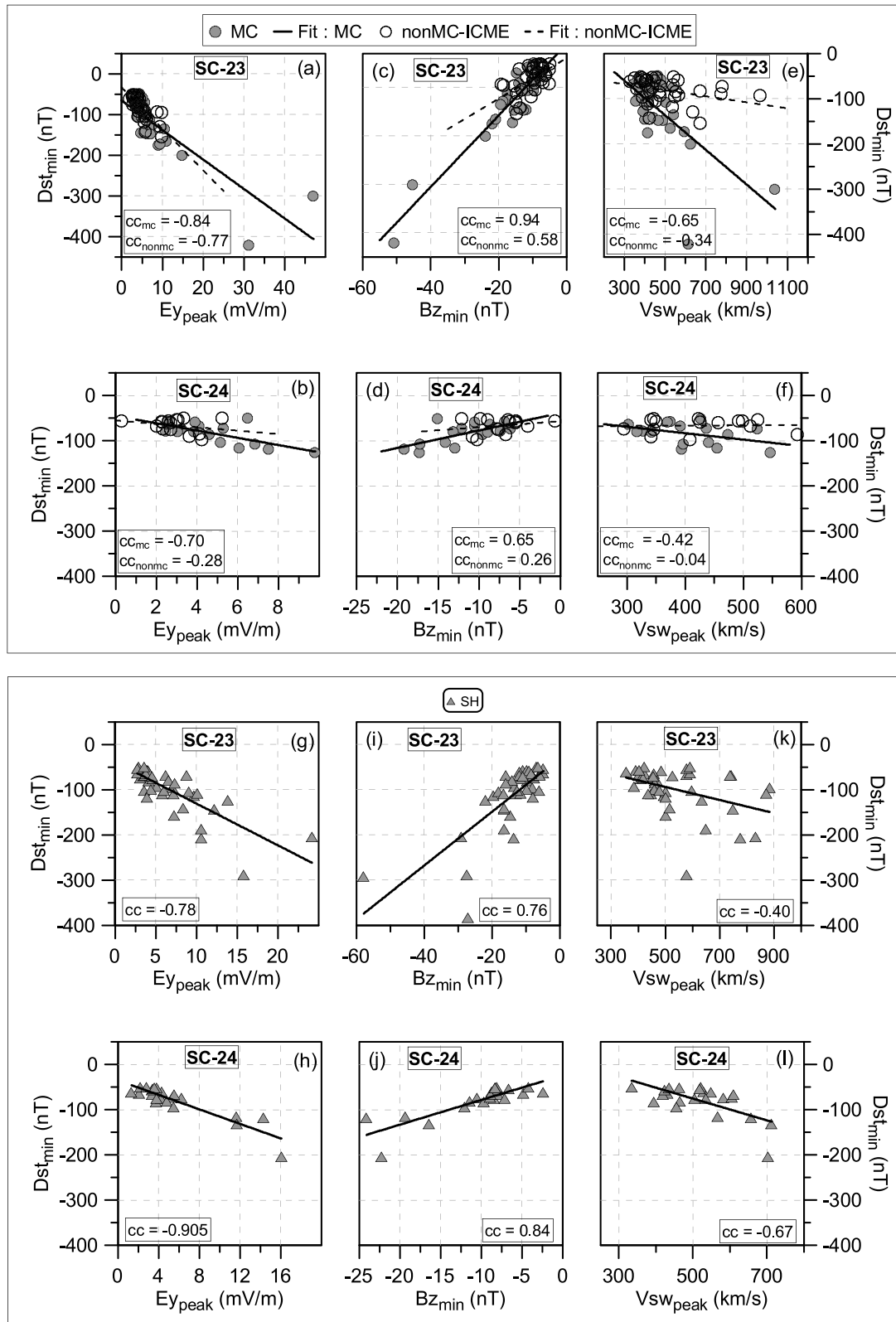


Figure 7. Scatter plots of Dst_{min} with Ey_{peak} , Bz_{min} , and Vsw_{peak} for the major solar wind-interplanetary drivers: (a–f) MC (closed circles) and (g–l) non-MC-ICME (open circles) SH during all the 135 storms ($Dst \leq -50$ nT) between December 2008 and December 2016. MC = magnetic cloud; ICME = interplanetary coronal mass ejection; SC = solar cycle.

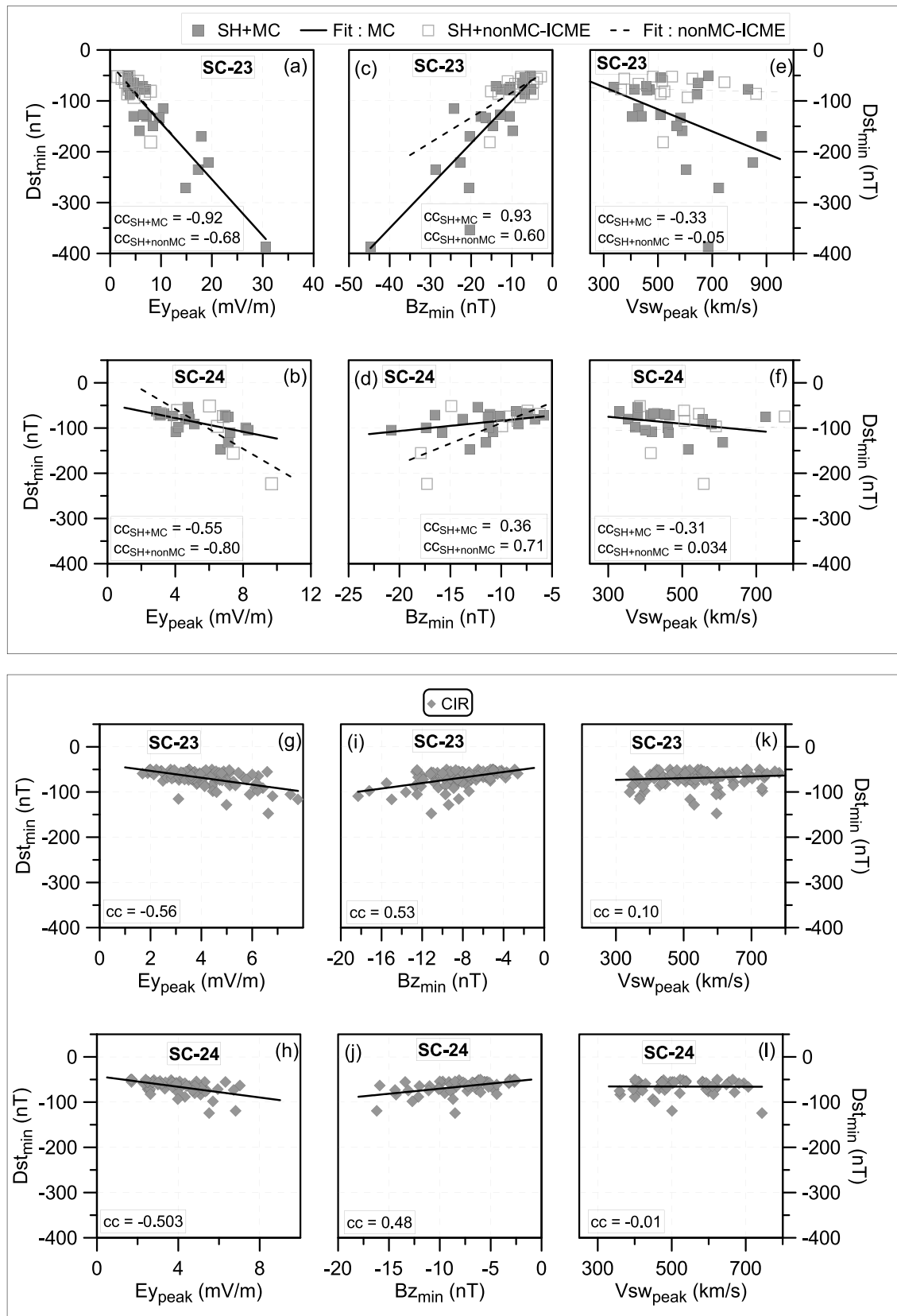


Figure 8. Same format as Figure 7 but for different drivers: (a–f) SH+MC (closed squares) and (g–l) SH+MC-ICME (open squares) and CIR.

Noteworthy is the high anticorrelations during ADP-24 storms between $E_{y_{\text{peak}}}$ and Dst_{min} for MC ($cc = -0.70$) panel (b), SH ($cc = -0.905$) panel (h), and SH+ICME ($cc = -0.8$) panel (n). CIR-driven storms show low correspondence ($cc = -0.50$) between $E_{y_{\text{peak}}}$ and Dst_{min} panel (f). For the correlations during ADP-23, we found high correspondences between $E_{y_{\text{peak}}}$ and Dst_{min} for ICME (a), SH (g), and SH+ICME (m)-driven storms (text labels in Figure 7). Best correspondence ($cc = -0.92$) was exhibited by SH+MC-driven storms.

E_y is a product of B_z and V_{sw} ; hence, correlation of the two latter parameters with Dst_{min} will be significant to ascertain geomagnetic activity levels. We obtained similar results for the correlations between $B_{z_{\text{min}}}$ and Dst_{min} for ADP-23 (panels c, i, and o) and ADP-24 (panels d, j, and p), as found for $E_{y_{\text{peak}}}$ and Dst_{min} correspondence. The ADP-24 storm correlations are high for the events driven by MC ($cc = 0.65$), SH ($cc = 0.84$), and SH+ICME ($cc = 0.71$), while for CIR-driven storms, correlation coefficient value dropped to 0.48 (panel k). Best correlation ($cc = 0.92$) between $B_{z_{\text{min}}}$ and Dst_{min} for ADP-23 is obtained for MC and SH+MC-driven storms. In contrast, for ADP-24 SH-driven storms exhibit best ($cc = 0.84$) $B_{z_{\text{min}}}$ and Dst_{min} correspondence.

The lower correlation for CIR-driven events could be attributed to the fluctuating CIR fields, which do not maintain southward orientation for long and do not attain large values in particular when compared to ICMEs (Gonzalez et al., 1999, 2011), and hence, magnetic reconnection with Earth's magnetopause leads only to weak and moderate intensity storms in case of CIRs (Tsurutani, 2006)

Correlation analysis carried out for $V_{sw_{\text{peak}}}$ and Dst_{min} does not show any well-defined pattern, but it is to be noted that moderate and intense storm events have wide range of $V_{sw_{\text{peak}}}$. This may be because most of the moderate storms are driven by CIRs and the intense storms drivers like SH, ICME, and SH+ICME also exhibit broad velocity range. The best correlation for ADP-24 between $V_{sw_{\text{peak}}}$ and Dst_{min} is exhibited in case of SH-driven storms ($cc = -0.67$), followed by MC ($cc = -0.42$), while for all other drivers there is weak correspondence ($cc > -0.1$). In contrast, for ADP-23 MC-driven storms show best correspondence between $V_{sw_{\text{peak}}}$ and Dst_{min} .

Hence, our study reaffirms the pivotal role of presence of significant E_y and B_z values for moderate and intense storms. We obtained that majority of the intense storms have $E_{y_{\text{peak}}} > 5$ mV/m, in contrast to the moderate storms, which have varying $E_{y_{\text{peak}}}$ values. Also, we found that 17 out of the total 18 intense storms have minimum B_z values < -10 nT. Hence, our results closely follow the criteria proposed by Gonzalez and Tsurutani (1987) for intense geomagnetic activity, which state that large southward B_z (≤ -10 nT) with $E_y > 5$ mV/m are the necessary interplanetary conditions for driving the intense geomagnetic storms. Another noteworthy point from the correlation analysis carried out above (Figure 7) is that MC and SH stand out as the most geoeffective structures, followed by SH+ICME during ADP-24.

4. Conclusions

1. We compare the ascending to EDPs of the two consecutive SCs 23 and 24, covering periods between May 1996 to July 2004 and December 2008 to December 2016, respectively. A striking difference obtained between the two periods is the occurrence rate of intense geomagnetic storms. While SC-24 witnessed only 18 intense geomagnetic storms during first 8 years, SC-23 witnessed 74 intense events during the same duration, out of which 8 were super-intense events ($Dst \leq -250$ nT), thus giving the intense storm occurrence rate of 2.2 storms per year in ADP-24, in contrast to ~ 9 storms per year in ADP-23. It is to be pointed out that ADP-24 did not witness any super-intense event.

Thus, the intense geomagnetic storm occurrence rate during ADP-24 was reduced nearly by a factor of 4 of that during ADP-23. During ADP-24, the lowest Dst_{min} value attained among the 18 intense events was $-4,223$ nT, in contrast to lowest Dst_{min} value of -422 nT among 74 intense storms of ADP-23. Moderate geomagnetic storm occurrence rate in the previous SC (23), on the other hand, was about 51% (~ 1.5 times) higher than that in the current cycle (24).

2. A comparative analysis between the solar wind plasma and magnetic field conditions during ADP-23 and ADP-24 depicts distinctly weaker SC 24 as compared to the previous cycle 23. During complete ADP-24, B_s was weaker than that in ADP-23. To determine the occurrences of geoeffective B_s and E_y , we computed the fraction of points with $B_s \geq 5$, $B_s \geq 10$, and $B_s \geq 20$ nT during both the periods (ADP-23 and ADP-24). We obtain the ratios of three respective cutoffs for ADP-23 to ADP-24 to be 1.5, 1.8, and 8.5, respectively. Similarly, the three thresholds for E_{dusk} ($E_{\text{dusk}} \geq 2.5$, $E_{\text{dusk}} \geq$, and $E_{\text{dusk}} \geq 12$ mV/m) showed that the ratios between ADP-23 to ADP-24 are 1.8, 2.3, and 10, respectively. The reduced occurrence of strong B_s and E_y in cycle 24 compared to cycle 23 probably contributed to the fewer moderate or intense storms in cycle 24.

3. ADP-24 clearly follows the dual peak characteristic in the moderate and intense storm occurrence rates. One of the peaks in storm occurrence was observed around late ascending phase period (year 2012). The second peak was witnessed during EDP (May–December 2016).
4. Seasonal distribution during ADP-24 exhibited no significant difference in the intense storm occurrence during vernal and equinoctial months. On the other hand, for ADP-23, there was an increase in the number of intense geomagnetic storms by a factor of 2 during autumnal equinox in comparison to vernal. Moderate geomagnetic storms did not exhibit much difference during ADP-23 and ADP-24. SC-24 witnessed fewer intense storms, and therefore, statistics might not be robust to make a definitive conclusion about their seasonal variation.
5. Investigation of the possible SW-IP drivers causing the moderate and intense geomagnetic storms during ADP-24 has revealed that about 41% of the moderate storms were driven by CIRs, whereas ICMEs and/or their SH contributed about 49%. In contrast, during ADP-23, 48% storms were CIR driven, while 41.3% were driven by ICME and/or their SH.
The intense storms during ADP-24, on the other hand, were mostly driven by ICMEs and/or their SH (~89%), in contrast, CIRs caused only 11% of the intense storms. For ADP-23, 64% were caused by ICMEs and/or their SH and about 13% were CIR driven.
During the complete ADP-24, the prevalence of CIR-driven geomagnetic storms in the rising phase (~47%) and important contribution during maximum (23.5%) and EDPs (~56%) is strikingly distinct feature of SC-24.

Acknowledgments

The authors wish to thank the anonymous referees for their invaluable and constructive comments. R. R. would like to thank Fundação de Amparo à Pesquisa do Estado de São Paulo (FAPESP) for financial support at INPE, Brazil, through postdoctoral research fellowship (2012/12049-1). Part of this revision work was supported by Council of Scientific and Industrial Research (CSIR) under the Senior Research Associate (Scientist's Pool) scheme (13(8871-A)/2016-Pool) at NCAOR contribution 38/2018, Goa. R. R. would like to thank Director, NCAOR, Goa, India for support. E. E. extends thanks to the Conselho Nacional de Desenvolvimento Científico e Tecnológico (CNPQ) for the support under project CNPq/PQ 302583/2015-7. The OMNI data were obtained from the GSFC/SPDF OMNIWeb interface at <http://omniweb.gsfc.nasa.gov>. Authors are thankful to the OMNI data team. We thank the WDC for Geomagnetism, Kyoto, for providing the geomagnetic activity indices. We extend thanks to the sunspot data source: WDC-SILSO, Royal Observatory of Belgium, Brussels.

References

- Ahn, B.-H., Kroehl, H. W., Kamide, Y., & Kihn, E. A. (2000). Seasonal and solar cycle variations of the auroral electrojet index. *Journal of Atmospheric and Solar - Terrestrial Physics*, *62*, 1301.
- Alves, M. V., Echer, E., & Gonzalez, W. D. (2006). Geoeffectiveness of corotating interaction regions as measured by *Dst* index. *Journal of Geophysical Research*, *111*, A07S05. <https://doi.org/10.1029/2005JA011379>
- Antalova, A., & Gnevyshev, M. N. (1965). Principal characteristics of the 11-year solar activity cycle. *Astronomicheskii Zhurnal*, *42*(2), 253–258.
- Borovsky, J. E., & Denton, M. H. (2006). Differences between CME-driven storms and CIR-driven storms. *Journal of Geophysical Research*, *111*, A07S08. <https://doi.org/10.1029/2005JA011447>
- Bothmer, V., & Zhukov, A. (2007). The Sun as the prime source of space weather, *Space weather—Physics and effects* (Chap. 3, pp. 31–102). Berlin: Springer.
- Burlaga, L. F., Mariani, S. F., & Schwenn, R. (1981). Magnetic loop behind an interplanetary shock: Voyager, Helios and IMP8 observations. *Journal of Geophysical Research*, *86*, 6673–6684.
- Burton, R. K., McPherron, R. L., & Russell, C. T. (1975). An empirical relationship between interplanetary conditions and *Dst*. *Journal of Geophysical Research*, *80*, 4204–4214.
- Cane, H. V., & Richardson, I. G. (2003). Interplanetary coronal mass ejections in the near-Earth solar wind during 1996–2002. *Journal of Geophysical Research*, *108*(A4), 1156. <https://doi.org/10.1029/2002JA009817>
- Chapman, S., & Bartels, J. (1940). *Geomagnetism* (Vol. 2). London: Oxford Univ. Press.
- Chen, H., Zhang, J., Ma, S., Yang, S., Li, L., Huang, X., & Xiao, J. (2015). Confined flares in solar active region 12192 from 2014 October 18 to 29. *Astrophysics Journal Letter*, *808*, L24. <https://doi.org/10.1088/2041-8205/808/1/L24>
- Cliver, E. W., Kamide, Y., & Ling, A. G. (2000). Mountains versus valleys: Semiannual variation of geomagnetic activity. *Journal of Geophysical Research*, *105*, 2413–2424. <https://doi.org/10.1029/1999JA900439>
- Cortie, A. L. (1912). Sun-spots and terrestrial magnetic phenomena, 1898–1911: The cause of the annual variation in magnetic disturbances. *Monthly Notices of the Royal Astronomical Society*, *73*, 52–60.
- De Toma, G. (2011). Evolution of coronal holes and implications for high-speed solar wind during the minimum between cycles 23 and 24. *Solar Physics*, *274*, 195–217. <https://doi.org/10.1007/s11207-010-9677-2>
- Dungey, J. R. (1961). Interplanetary magnetic field and auroral zones. *Physical Review Letters*, *6*, 47–48.
- Echer, E., Gonzalez, W. D., & Tsurutani, B. T. (2011). Statistical studies of geomagnetic storms with peak *Dst* ≤ −50 nT from 1957 to 2008. *Journal of Atmospheric and Solar - Terrestrial Physics*, *73*, 1454–1459.
- Echer, E., Gonzalez, W. D., Tsurutani, B. T., & Gonzalez, A. L. C. (2008). Interplanetary conditions causing intense geomagnetic storms (*Dst* ≤ −100 nT) during solar cycle 23 (1996–2006). *Journal of Geophysical Research*, *113*, A05221. <https://doi.org/10.1029/2007JA012744>
- Echer, E., Tsurutani, B. T., & Gonzalez, W. D. (2012). Extremely low geomagnetic activity during the recent deep solar cycle minimum. *Proceedings of the International Astronomical Union*, *7*, 200–209. <https://doi.org/10.1017/S174392131200484X>
- Echer, E., Tsurutani, B. T., & Gonzalez, W. D. (2013). Interplanetary origins of moderate (−100 nT < *Dst* ≤ −50 nT) geomagnetic storms during solar cycle 23 (1996–2008). *Journal of Geophysical Research, Space Physics*, *118*, 385–392. <https://doi.org/10.1029/2012JA018086>
- Feminella, F., & Storini, M. (1997). Large-scale dynamical phenomena during solar activity cycles. *Astronomy and Astrophysics*, *322*(1), 311–319.
- Gazis, P. R. (1996). Solar cycle variation in the heliosphere. *Reviews of Geophysics*, *34*, 379–402.
- Gibson, S. E., Kozyra, J. U., de Toma, G., Emery, B. A., Onsager, T., & Thompson, B. J. (2009). If the Sun is so quiet, why is the Earth ringing? A comparison of two solar minimum intervals. *Journal of Geophysical Research*, *114*, A09105. <https://doi.org/10.1029/2009JA014342>
- Gnevyshev, M. N. (1963). The corona and the 11-year cycle of solar activity. *Soviet Astronomy - AJ*, *7*(3), 311–318.
- Gnevyshev, M. N. (1967). On the 11-years cycle of solar activity. *Solar Physics*, *1*, 107–120. <https://doi.org/10.1007/BF00150306>
- Gonzalez, W. D., Echer, E., Gonzalez, A. L. C., & Tsurutani, B. T. (2007). Interplanetary origin of intense geomagnetic storms (*Dst* < −100 nT) during solar cycle 23. *Geophysical Research Letters*, *34*, L06101. <https://doi.org/10.1029/2006GL028879>
- Gonzalez, W. D., Echer, E., Gonzalez, A. L. C., Tsurutani, B. T., & Lakhina, G. S. (2011). Extreme geomagnetic storms, recent Gleissberg cycles and space era-super intense storms. *Journal of Atmospheric and Solar - Terrestrial Physics*, *73*, 1447–1453.

- Gonzalez, W. D., Gonzalez, A. L. C., & Tsurutani, B. T. (1990). Dual-peak solar cycle distribution of intense geomagnetic storms. *Planetary and Space Science*, *38*, 181–187.
- Gonzalez, W. D., Joselyn, J. A., Kamide, Y., Kroehl, H. W., Rostoker, G., Tsurutani, B. T., & Vasyliunas, V. (1994). What is a geomagnetic storm? *Journal of Geophysical Research*, *99*, 5771–5792.
- Gonzalez, W. D., & Tsurutani, B. T. (1987). Criteria of interplanetary parameters causing intense magnetic storms ($Dst \leq -100$ nT). *Planetary and Space Science*, *35*, 1101.
- Gonzalez, W. D., Tsurutani, B. T., & Gonzalez, A. L. C. (1999). Interplanetary origin of geomagnetic storms. *Space Science Reviews*, *88*, 529–562. <https://doi.org/10.1023/A:1005160129098>
- Gopalswamy, N., Yashiro, S., Xie, H., Akiyama, S., & Mäkelä, P. (2015). Properties and geoeffectiveness of magnetic clouds during solar cycles 23 and 24. *Journal of Geophysical Research: Space Physics*, *120*, 9221–9245. <https://doi.org/10.1002/2015JA021446>
- Hajra, R., Echer, E., Tsurutani, B. T., & Gonzalez, W. D. (2013). Solar cycle dependence of high-intensity long-duration continuous AE activity (HILDCAA) events, relativistic electron predictors. *Journal of Geophysical Research: Space Physics*, *118*, 5626–5638. <https://doi.org/10.1002/jgra.50530>
- Hathaway, D. H. (2010). The solar cycle. *Living Reviews in Solar Physics*, *7*, 1.
- Huttunen, K. E. J., Koskinen, H. E. J., & Schwenn, R. (2002). Variability of magnetospheric storms driven by different solar wind perturbations. *Journal of Geophysical Research*, *107*(A7), 1121. <https://doi.org/10.1029/2001JA900171>
- Kan, J. R., & Lee, L. C. (1979). Energy coupling function and solar windmagnetosphere dynamo. *Geophysical Research Letters*, *6*, 577–580.
- Kilpua, E. K. J., Luhmann, J. G., Jian, L. K., Russell, C. T., & Li, Y. (2014). Why have geomagnetic storms been so weak during the recent solar minimum and the rising phase of cycle 24. *Journal of Atmospheric and Solar - Terrestrial Physics*, *107*, 12–19. <https://doi.org/10.1016/j.jastp.2013.11.001>
- Lepping, R. P., Wu, C., & Berdichevsky, D. B. (2015). Yearly comparison of magnetic cloud parameters, sunspot number, and interplanetary quantities for the first 18 years of the wind mission. *Solar Physics*, *290*, 553–578. <https://doi.org/10.1007/s11207-014-0622-7>
- Lyatsky, W., Newell, P. T., & Hamza, A. M. (2001). Solar illumination as cause of the equinoctial preference for geomagnetic activity. *Geophysical Research Letters*, *28*, 2353–2356.
- McComas, D. J., Barraclough, B. L., Funsten, H. O., Gosling, J. T., Santiago-Muñoz, E., Skoug, R. M., et al. (2000). Solar wind observations over Ulysses' first full polar orbit. *Journal of Geophysical Research*, *105*(A5), 10419–10433. <https://doi.org/10.1029/1999JA000383>
- Mursula, K., Tanskanen, E., & Love, J. J. (2011). Spring-fall asymmetry of substorm strength, geomagnetic activity and solar wind: Implications for semiannual variation and solar hemispheric asymmetry. *Geophysical Research Letters*, *38*, L06104. <https://doi.org/10.1029/2011GL046751>
- Norton, A. A., & Gallagher, J. C. (2010). Solar-cycle characteristics examined in separate hemispheres: Phase, Gnevyshev Gap, and length of minimum. *Solar Physics*, *261*, 193.
- Oh, S. Y., & Yi, Y. (2011). Solar magnetic polarity dependency of geomagnetic storm seasonal occurrence. *Journal of Geophysical Research*, *116*, A06101. <https://doi.org/10.1029/2010JA016362>
- Priester, W., & Catanni, D. (1962). On the semiannual variations of geomagnetic activity and its relations to the solar corpuscular radiation. *Journal of Atmospheric and Solar - Terrestrial Physics*, *19*, 121–126.
- Rawat, R., Alex, S., & Lakhina, G. S. (2010). Storm-time characteristics of intense geomagnetic storms ($Dst \leq -200$ nT) at low-latitudes and associated energetics. *Journal of Atmospheric and Solar - Terrestrial Physics*, *72*, 1364–1371. <https://doi.org/10.1016/j.jastp.2010.09.029>
- Richardson, I. G. (2013). Geomagnetic activity during the rising phase of solar cycle 24. *Journal Space Weather Space Climate*, *3*, A08. <https://doi.org/10.1051/swsc/2013031>
- Richardson, I. G., & Cane, H. V. (2012b). Near-earth solar wind flows and related geomagnetic activity during more than four solar cycles (1963–2011). *Journal Space Weather Space Climate*, *2*, A02. <https://doi.org/10.1051/swsc/2012003>
- Richardson, I. G., Webb, D. F., Zhang, J., Berdichevsky, D. B., Biesecker, D. A., Kasper, J. C., et al. (2006). Major geomagnetic storms ($Dst \leq -100$ nT) generated by corotating interaction regions. *Journal of Geophysical Research*, *111*, A07509. <https://doi.org/10.1029/2005JA011476>
- Russell, C. T., & McPherron, R. L. (1973). Semiannual variation of geomagnetic activity. *Journal of Geophysical Research*, *78*, 92–108.
- Saiz, E., Cerrato, Y., Cid, C., Dobrica, V., Hejda, P., Nenovski, P., et al. (2013). Geomagnetic response to solar and interplanetary disturbances. *Journal Space Weather Space Climate*, *3*, A26. <https://doi.org/10.1051/swsc/2013048>
- Schwabe, H. (1844). Sonnen-beobachtungen im Jahre 1843. *Astronomische Nachrichten*, *21*(495), 233–236.
- Selvakumaran, R., Veenadhari, B., Akiyama, S., Pandya, M., Gopalswamy, N., Yashiro, S., et al. (2016). On the reduced geoeffectiveness of solar cycle 24: A moderate storm perspective. *Journal of Geophysical Research: Space Physics*, *121*, 8188–8202. <https://doi.org/10.1002/2016JA022885>
- Shanmugaraju, A., Syed Ibrahim, M., Moon, Y., et al. (2015). Empirical relationship between CME parameters and geo-effectiveness of Halo CMEs in the rising phase of Solar Cycle 24 (2011–2013). *Solar Physics*, *290*, 1417–1427. <https://doi.org/10.1007/s11207-015-0671-6>
- Sheeley, N. R. Jr., & Wang, Y.-M. (2015). The recent rejuvenation of the Sun's large-scale magnetic field: A clue for understanding past and future sunspot cycles. *Astronomy Journal*, *809*, 113. <https://doi.org/10.1088/0004-637X/809/2/113>
- Shen, C., Chi, Y., Wang, Y., Xu, M., & Wang, S. (2017). Statistical comparison of the ICME's geoeffectiveness of different types and different solar phases from 1995 to 2014. *Journal of Geophysical Research: Space Physics*, *122*, 5931–5948. <https://doi.org/10.1002/2016JA023768>
- Storini, M., Bazilevskaya, G. A., Flueckiger, E. O., et al. (2003). The Gnevyshev gap: A review for space weather. *Advances in Space Research*, *31*, 895–900.
- Storini, M., & Pase, S. (1995). Long term solar features derived from polar looking cosmic ray detectors. In *Proceedings of 2nd SOLTIP Symposium, Nakaminato, 1, Special Issue of STEP — GBRSC NewsT. Watanabe* (pp. 255–258). Japan: Ibaraki University Mito.
- Storini, M., Pase, S., Sýkora, J., & Parisi, M. (1997). Two components of cosmic-ray modulation. *Solar Physics*, *172*, 317–325.
- Sugiura, M. (1964). Hourly values of equatorial Dst for IGY. *Annual International Geophysics Year*, *35*, 9.
- Sun, X., Bobra, M. G., Hoeksema, J. T., Liu, Y., Li, Y., Shen, C., et al. (2015). Why is the great solar active region 12192 flare-rich but CME-poor? *Astrophysics Journal Letter*, *804*, L28. <https://doi.org/10.1088/2041-8205/804/2/L28>
- Tsurutani, B. T. (2006). Corotating solar wind streams and recurrent geomagnetic activity: A review. *Journal of Geophysical Research*, *111*, A07501. <https://doi.org/10.1029/2005JA011273>
- Tsurutani, B. T., Echer, E., & Gonzalez, W. D. (2011). The solar and interplanetary causes of the recent minimum in geomagnetic activity (MGA23): A combination of midlatitude small coronal holes, low IMF BZ variances, low solar wind speeds and low solar magnetic fields. *Annales de Geophysique*, *29*, 839–849. <https://doi.org/10.5194/angeo-29-839-2011>
- Tsurutani, B. T., & Gonzalez, W. D. (1997). The interplanetary causes of magnetic storms: A review. In B. T. Tsurutani (Ed.), *Magnetic storms, geophysics monograph series* (Vol. 98, pp. 77). Washington, DC: AGU. <https://doi.org/10.1029/GM098p0077>

- Tsurutani, B. T., Gonzalez, W. D., Tang, F., Akasofu, S. I., & Smith, E. J. (1988). Origin of interplanetary southward magnetic fields responsible for major magnetic storms near solar maximum (1978–1979). *Journal of Geophysical Research*, *93*(A8), 8519–8531. <https://doi.org/10.1029/JA093iA08p08519>
- Wang, Y.-M., & Sheeley, N. R. Jr. (2015). Coronal mass ejections and the solar cycle variation of the Sun's open flux. *Astrophysics Journal Letter*, *809*, L24. <https://doi.org/10.1088/2041-8205/809/2/L24>
- Wang, Y., Shen, C. L., Wang, S., & Ye, P. Z. (2003). An empirical formula relating the geomagnetic storm's intensity to the interplanetary parameters: $-\overline{V B_z}$ and ∇t . *Geophysical Research Letters*, *30*(20), 2039. <https://doi.org/10.1029/2003GL017901>
- Yermolaev, Y. I., Nikolaeva, N. S., Lodkina, I. G., & Yermolaev, M. Y. (2012). Geoeffectiveness and efficiency of CIR, sheath, and ICME in generation of magnetic storms. *Journal of Geophysical Research*, *117*, A00L07. <https://doi.org/10.1029/2011JA017139>
- Zhang, J., Richardson, I. G., Webb, D. F., Gopalswamy, N., Huttunen, E., Kasper, J. C., et al. (2007). Solar and interplanetary sources of major geomagnetic storms ($Dst \leq -100$ nT) during 1996–2005. *Journal of Geophysical Research*, *112*, A10102. <https://doi.org/10.1029/2007JA012321>
- Zhao, H., & Zong, Q.-G. (2012). Seasonal and diurnal variation of geomagnetic activity: Russell-Mcpherron effect during different IMF polarity and/or extreme solar wind conditions. *Journal of Geophysical Research*, *117*, A11222. <https://doi.org/10.1029/2012JA017845>
- Zieger, B., & Mursula, K. (1998). Annual variation in near-Earth solar wind speed: Evidence for persistent north-south asymmetry related to solar magnetic polarity. *Geophysical Research Letters*, *25*, 841–844.